A kernel induced energy based active contour method for image segmentation

Xiaofeng Li[1*], Yanfang Yang[1], Limin Jia[2]

[1]*School of Traffic and Transportation, Beijing Jiaotong University, No.3, Shang Yuan Cun, Haidian District, Beijing, China*

[2]*State Key Laboratory of Rail Traffic Control and Safety, Beijing Jiaotong University, No.3, Shang Yuan Cun, Haidian District, Beijing, China*

Received 4 March 2014, www.tsi.lv

Abstract

Active contour model is a promising method in image segmentation. However, existing active contour model and its evolution often suffer from slower convergence rates and easily to be trapped in local optima due to the presence of noise. In this paper, a novel curve evolution model based on kernel mapping method is presented. The method first transforms original image data into a kernel-induced space by a kernel function. In the kernel-induced space, the kernel-induced non-Euclidean distance between the observations and the regions parameters is integrated to formulate a new level set based active contour model. The method proposed in this paper leads to a flexible and effective alternative to complex model the image data. In the end of this paper, detailed experiments are given to show the effectiveness of the method in comparison with conventional active contour model methods.

Keywords: Kernel mapping; Active contour; Chan-Vese model; Level-set; Image segment

1 Introduction

Object boundary detection is a key of the fundamental process in image processing that facilitates higher level image analysis, description, recognition and visualization of objects of interest. Realizing the importance of object boundary detection in image processing, a great number of breakthroughs have been made in the past several decades. However, Object boundary detection remains actually problem-centric. Achieving a generic detection method that is universally applicable for broad range of problem domains is difficult [1].

Active contour models have been extensively studied and used in object boundary detection, once it was introduced by Kass et al [2]. However the technique requires the initial con- tour to lie outside the feature of interest and relies on an inherent contraction force to move the contour towards the feature. Cohen [3, 4] proposed an inflating contour that reduced the sensitivity to initialization. Geodesic active contour model [5]-[9], which is the original snake model in level-set frame, allows changes in topology. Other implementations have also been proposed for capturing more global minimizers by restricting the search space. Dual snakes [10] and dual-band active contour [11] restrict their search spaces exploiting normal lengths on the initial contour. Using of simulated annealing for minimization [12] and dynamic programming [13] has been integrated into the snake model.

All these classical snakes and active contour models rely on image gradient to stop the curve evolutions. Thus the performance of the purely edge-based models is often inadequate. Complex region-based energy functional are researched to likely to yield undesirable local minima when compared to simpler edge-energy functional.

Region-based models have many advantages over edge-based ones. First region-based models utilize image information not only near the evolving contour, but also statistical information inside and outside the contour, which are less sensitive to noise and have better performance for images with weak edges or without edges. Second, they are significantly less sensitive to the location of initial contour then can efficiently detect the exterior and interior boundaries simultaneously. One of the most popular region-based models is the Chan-Vese model [14], inspired by Mumford-Shah functional [15]. This model, as well as most of the region-based energy functional, is computationally onerous.

In order to overcome the limitations, especially the high computational cost, clustering of data is integrated into image segmentation. Vazquez et al [16] showed that image segmentation is spatially constrained clustering of image data. Gibou et al. [17] utilized the simplicity of the k-means algorithm, however, the main drawback is that they are more sensitive to noise.

This paper deals with the above mentioned problems. It presents a novel kernel induced-based active contour, which can handle objects whose boundaries are not necessarily defined by gradient, objects with very smooth

[*]***Corresponding author*** e-mail: xfengli@bjtu.edu.cn

or even with discontinuous boundaries. Salah et al [18], [19] show that kernel mapping is quite effective in segmentation of various types of images. The kernel function maps implicitly the original image data into a kernel space in a higher dimension and, then, a simpler method in induced space will be possible [20]. The mapping, which transforms the original image data in a higher dimensional space, is implicitly. The transformed data in a higher dimensional space can be expressed via the kernel function because the dot product, the Euclidean norm thereof. The kernel induced method is a tool that has been intensively used in data clustering, but not in active contour methods. Generally, kernel induced methods provide more accurate and robust data clustering, thus, we combine it with active contour methodology, introducing here a model as a kernel induced space-based minimization. The kernel induced method of the energy provides a balanced technique with strong ability to reject "weak" local minima. We use a common kernel function, the radial basis function (RBF), in this paper, and then verify the effectiveness of the method by a quantitative and comparative performance evaluation to Chan-Vese model over a large number of experiments on synthetic images, as well as diverse real image

The remainder of the paper is organized as follows: The description of the model, its kernel induced motivation energy and its properties are presented in Section II. Experimental results are presented in Section III and conclusions are drawn in Section IV.

2 Description of model

2.1 PROPOSED MODEL

The basic idea of the model will be introduced in this section. The image data is generally non-linearly separable. The advantage of kernel mapping is that it maps implicitly the original image data into a kernel space in a higher dimension and, then, a simpler methods in induced space will be possible. In this section, we transform the image data implicitly via a kernel function firstly, and, then, use a kernel-induced non Euclidian distances to form the minimizing functional. To explain the role of the kernel mapping in the segmentation functional proposed in this paper, and describe clearly the ensuing algorithm, we first assume that the original image is formed by two regions of approximately piecewise-constant intensities.

Let $\varphi(\cdot)$ be a non-linear mapping from the observation space $\mathcal{I}$ to a higher (possibly infinite) dimensional feature space $\mathcal{F}$. Let us defined the evolving the curve C in the image domain Ω. As assumed above, the image I is formed by two regions of approximately piecewise-constant intensities, of distinct values I_1 and I_2. Assume that the object to be detected is represented by the region with the value I_1, and its boundary by C_0. So we have $I \approx I_1$ inside the object (inside C_0) and $I \approx I_2$ outside the object (outside C_0). Now let us consider the following functional:

$$\begin{aligned} F_1(C)+F_2(C) &= \int_{inside(C)} \left\|\varphi(I(x,y))-\varphi(c_1)\right\|^2 dxdy \\ &+\int_{outside(C)} \left\|\varphi(I(x,y))-\varphi(c_2)\right\|^2 dxdy \end{aligned}, \quad (1)$$

where c_1 and c_2 are regions parameters depending on C. The energy terms $F_i(C)$ measure a kernel-induced non Euclidian distances between the observations and the regions parameters c_i, $i=1,2$.

Following the Mercer's theorem conditions [20], the explicit mapping φ has not been known. Instead, the transformed data can be expressed via a continuous, symmetric, positive semi-definite kernel function $K(x,y)$:

$$K(x.y)=\varphi(x)^T\cdot\varphi(y),\ \forall(x,y)\in\mathcal{I}^2, \quad (2)$$

where "$\cdot$" is the dot product in the feature space $\mathcal{F}$. Substitution of the kernel functions gives, for $c_i \in \{c_1,c_2\}$:

$$\begin{aligned} J_K(I(x,y),c_i) &= \left\|\varphi(I(x,y))-\varphi(c_i)\right\|^2 \\ &= (\varphi(I(x,y))-\varphi(c_i))^T\cdot(\varphi(I(x,y))-\varphi(c_i)) \\ &= K(I(x,y),I(x,y))+K(c_i,c_i)-2K(I(x,y),c_i) \end{aligned}, \quad (3)$$

where c_1 and c_2 are constants depending on C, expressing the average prototypes of the image regions inside and outside respectively of C. In this simple case, it is obvious that the boundary of the object C_0, is the minimizer of the fitting term:

$$\inf_C\{F_1(C)+F_2(C)\}\approx 0\approx F_1(C_0)+F_2(C_0). \quad (4)$$

The five cases are illustrated in Figure 1. If the curve C is outside the object, then $F_1(C)>0$ and $F_2(C)\approx 0$ or $F_1(C)\approx 0$ and $F_2(C)>0$ depending on object position (inside or outside the curve). If the curve C is inside the object, then $F_1(C)\approx 0$ and the $F_2(C)>0$. If C is both inside and outside the object, then $F_1(C)>0$ and the $F_2(C)>0$. Finally, the fitting term is minimized when $C=C_0$, i.e., when the curve C is on the boundary of the object. That is, the fitting term is minimized when the curve C is converged to the object boundary C_0.

FIGURE 1 All possible case in the position of the curve C in relation to the object under consideration

The proposed active contour is based on the minimization of the above fitting term, taking into account the length term of the model C as a regularization term. Therefore, the energy functional $F(C,c_1,c_2)$ is introduced as:

$$\begin{aligned} &F(C,c_1,c_2)=\mu\cdot Length(C)\\ &+\lambda_1\int_{inside(C)}\left\|\varphi(I(x,y))-\varphi(c_1)\right\|^2 dxdy\\ &+\lambda_2\int_{outside(C)}\left\|\varphi(I(x,y))-\varphi(c_2)\right\|^2 dxdy \end{aligned} . \quad (5)$$

In equation (5), $\mu\geq 0$, λ_1, $\lambda_2>0$ are fixed parameters. The curve C_0 that minimizes F

$$F(C_0,c_1,c_2)=\inf_C F(C,c_1,c_2). \quad (6)$$

Some common kernel functions are listed in Table I. In this paper, the radial basis function (RBF) kernel, which has been prevalent in pattern dada clustering [18, 22, 23] is adopted.

TABLE 1 Examples of prevalent kernel function

RBF Kernel	$K(x,y)=\exp(-\|x-y\|^2/\sigma^2)$
Sigmoid Kernel	$K(x,y)=\tanh(c(x\cdot y)+\theta)$
Polynomial Kernel	$K(x,y)=(x\cdot y+c)^d$

The radial basis function (RBF) kernel is given as:

$$K(x,y)=\exp(-\left\|x-y\right\|^2/\sigma^2). \quad (7)$$

With an RBF function, the equation (3), $J_K(I,c_i)$ can be simplified to $2(1-K(I(x,y),c_i))$, $i=1,2$. The necessary conditions for a minimum of F with respect to region parameters are:

$$c_i-gR_i(c_i)=0, i\in\{1,2\}, \quad (8)$$

where

$$\frac{\int_{R_i} I(x,y)K(I(x,y),c_i)dxdy}{\int_{R_i} K(I(x,y),c_i)dxdy},\ i\in\{1,2\}. \quad (9)$$

2.2 LEVEL-SET FORMULATION OF THE PROPOSED MODEL

In the level set formula, $C\subset\Omega$ is represented by the zero level set of a Lipschitz function $\phi:\Omega\to\mathbb{R}$, such that

$$\begin{cases} C=\{(x,y)\in\Omega:\phi(x,y)=0\}\\ inside(C)=\{(x,y)\in\Omega:\phi(x,y)>0\}\\ outside(C)=\{(x,y)\in\Omega:\phi(x,y)<0\} \end{cases}. \quad (10)$$

Using the Heaviside function H_ε, and the Dirac measure δ_ε as the regularized versions defined, respectively, by

$$\begin{cases} H_\varepsilon(z)=\frac{1}{2}(1+\frac{2}{\pi}\arctan(\frac{z}{\varepsilon})),\\ \delta_\varepsilon(z)=\frac{1}{\pi}\cdot\frac{\varepsilon}{\varepsilon^2+z^2}, \quad z\in R \end{cases}. \quad (11)$$

We express the terms in the energy F in the following way:

$$\begin{aligned} &Length\{\phi=0\}=\int_\Omega|\nabla H(\phi(x,y))|dxdy\\ &=\int_\Omega\delta_\varepsilon(\phi(x,y))|\nabla\phi(x,y)|dxdy \end{aligned}, \quad (12)$$

$$\begin{aligned} &\int_{inside(C)}\left\|\varphi(I(x,y))-\varphi(c_1)\right\|^2 dxdy\\ &=\int_\Omega\left\|\varphi(I(x,y)-\varphi(c_1))\right\|^2 H_\varepsilon(\phi)dxdy \end{aligned}. \quad (13)$$

In equation (13)

$$\begin{aligned} &\int_{outside(C)}\left\|\varphi(I(x,y))-\varphi(c_2)\right\|^2 dxdy\\ &=\int_\Omega\left\|\varphi(I(x,y)-\varphi(c_2))\right\|^2(1-H_\varepsilon(\phi))dxdy \end{aligned}. \quad (14)$$

Keeping the ϕ fixed and minimizing the energy $F(\phi,c_1,c_2)$ with respect to the constant c_1 and c_2, it is easy to express these constants function of ϕ by

$$c_1(\phi)=\frac{\int_\Omega I(x,y)K(I(x,y),c_i)H(\phi(x,y))dxdy}{\int_\Omega K(I(x,y),c_i)H(\phi(x,y))dxdy}, \quad (15)$$

$$c_2(\phi)=\frac{\int_\Omega I(x,y)K(I(x,y),c_i)(1-H(\phi(x,y)))dxdy}{\int_\Omega K(I(x,y),c_i)(1-H(\phi(x,y)))dxdy}. \quad (16)$$

The region term (13), (14) and the contour smoothness term in (12) are integrated into the energy function given by (5), producing

$$\begin{aligned} &F_\varepsilon(\phi,c_1,c_2)=\mu\int_\Omega\delta_\varepsilon(\phi)|\nabla\phi(x,y)|dxdy\\ &+\lambda_1\int_\Omega\left\|\varphi(I(x,y)-\varphi(c_1))\right\|^2 H_\varepsilon(\phi)dxdy\\ &+\lambda_2\int_\Omega\left\|\varphi(I(x,y)-\varphi(c_2))\right\|^2(1-H_\varepsilon(\phi))dxdy \end{aligned}. \quad (17)$$

Keeping c_1 and c_2 fixed and minimizing F_ε with respect to ϕ, we deduce the associated Euler-Lagrange equation for ϕ. Parameterizing the descent direction by an artificial time $t \geq 0$, the equation in $\phi(t,x,y)$ ($\phi(0,x,y)=\phi_0(x,y)$) defining the initial contour is

$$\frac{\partial \phi}{\partial t} = [\mu div(\frac{\nabla \phi}{|\nabla \phi|}) - \lambda_1 J_K(I(x,y),c_1) + \lambda_2 J_K(I(x,y),c_2)]\delta_\varepsilon(\phi) \quad (18)$$

3 Experimental results

In this section, we show the performance of the proposed method by presenting numerical results using the kernel-induced model on various synthetic and real images, with different types of contours and shapes. We show the active contour evolving in the original image Ω, and the associated piecewise-constant approximation of Ω (given by constant c_1 and c_2). In our numerical experiments, we generally choose the parameters to be $\lambda_1 = \lambda_2 = 1$. Only the length parameter μ is not same in our parameters. As shown in [24], μ plays a scaling role in the minimizing functions. μ should be small, if we have to detect all or as many objects as possible and of any size, and be lager when we have to detect large objects.

In the following, we illustrate the flexibility of the proposed method by a representative sample of the tests with various classes of real images and synthetic image with different noise models, and compare the computational time of different models.

Medical image segmentation is challenging and of a rapidly growing interest in recently years. Figure 2 illustrates that the proposed model can detect different objects of different intensities. Figure 2(a) depicts very narrow human vessels with very small contrast within some spots. The curves obtained at convergence are displayed, in Figure 3(f). Segmentation regions, represented by their parameters at convergence, are shown in Figure 2(f) and Figure 3(f). As shown in the two images, the length parameter in Figure 3 is larger than Figure 2, because the object of interest we have to detect, in Figure 3(a), is larger.

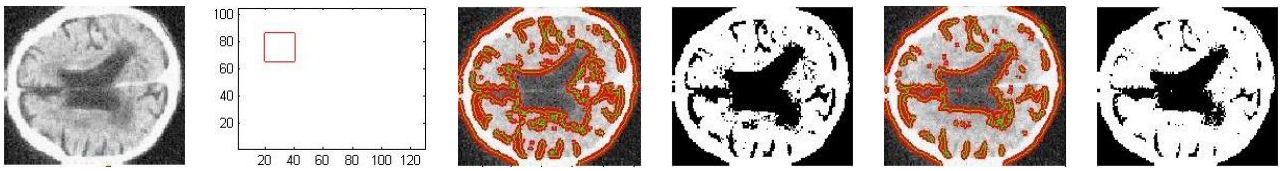

(a) (b) (c) (d) (e) (f)

FIGURE 2 (a):Brain images; (b): initialization; (c): final position of the curves with Chan-Vese model; (d): final segmentation with Chan-Vese model; (e): final position of the curves with proposed model; (f): final segmentation with proposed model. Image size: 100×120, $\mu = 0.1$

(a) (b) (c) (d) (e) (f)

FIGURE 3 (a): Vessel images; (b): initialization; (c): final position of the curves with Chan-Vese model; (d): final segmentation with Chan-Vese model; (e): final position of the curves with proposed model; (f): final segmentation with proposed model. Image size: 100×80, $\mu = 0.2$

The ability of the proposed model to deal with different noise models allows segmenting regions which require different models. To illustrate this important advantage of the proposed model, we consider a synthetic image with different noise models, as shown in Figure 4 (a), (b). Figure 4 (a) is generated with a salt and pepper noise, the corresponding noise density d is 0.1, the Gaussian noise is added in Figure 4 (b), the corresponding mean u is 0, the variance σ is 0.05. The final segmentation results with Chan-Vese model is in Figure 4 (a1-b2), and final segmentation results with proposed model, in Figure 4 (b1-b2). As shown in Figures 4 (a1-b2), the Chan-Vese model gives incorrect results as expected. The results demonstrate the ability of our kernel-induced method to insensitive to different noise models.

The computational time for the proposed model and the Chan-Vese model are shown in Table II. The proposed kernel-induced model achieves noticeably lower the Chan-Vese model in all of the medical images. In noisy images, the proposed model costs less time obviously compared to the Chan-Vese model, which demonstrates the ability of proposed model in handling noise.

Figure 5 and Figure 6 demonstrate how the proposed algorithm detects object boundaries on real images, and illustrate the robustness with respect to initial conditions, initial curves were either big rectangle placed arbitrarily about the middle of the image or tiny circles spread all over the image. Segmentation of a natural plane image into two regions is in Figure 5. Original, initial contour and final position of the evolving curve are displayed respectively in Figure 5 (a-c). The final segmentation regions, represented by their parameters at convergence, are illustrated in Figure 5(d). Figure 6 depicts how the proposed method, with the initial contour of tiny circles spread all over the image, detects the boundaries in real image.

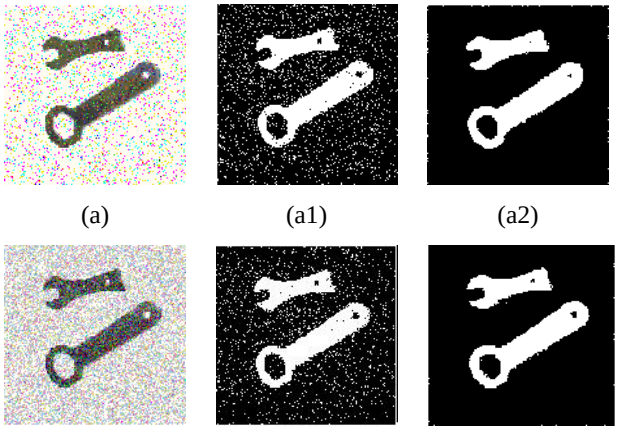

(a) (a1) (a2)

(b) (b1) (b2)

FIGURE 4 Image with different noise models: (a-b) image with salt & pepper , noise density $d = 0.1$ (first row) and Gaussian (second row) noises, mean $u = 0$ and variance $\sigma = 0.05$; (a1-b1) segmentation results with Chan-Vese model; (a2-b2) segmentation results with proposed model. Image size: 200×200 , $\mu = 0.12$

TABLE 2 Comparison of computation time (Seconds)

	Without noise		With noise	
Model	Brain	Vessel	Salt & Pepper noise	**Gaussian noise**
Proposed model	15.43	10.98	90.45	**61.73**
Chan-Vese model	**19.97**	**22.77**	**271.2**	**522.40**

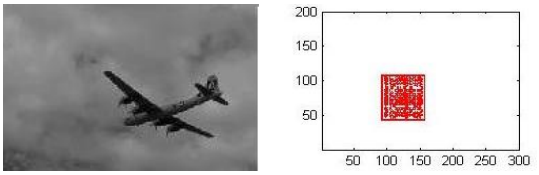

(a) (b)

(c) (d)

FIGURE 5 (a) Real plane image; (b) initialization; (c) final position of the curve; (d) final segmentation. Image size: 200×300 , $\mu = 0.1$

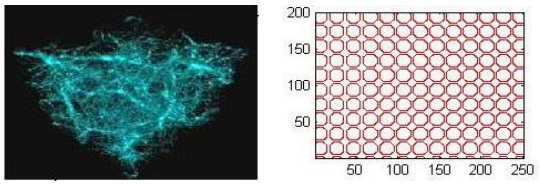

(a) (b)

(c) (d)

FIGURE 6 (a) Real image; (b) initialization; (c) final position of the curve; (d) final segmentation. Image size: 200×250 , $\mu = 0.02$

4 Conclusion

In this paper, a novel fast and robust model for active contours to detect objects in an image was introduced. The model can detect objects whose boundaries are not necessarily defined by gradient, due to the fact that it is based on an energy minimization algorithm, and not on an edge-function as the most classical active contour models. This energy is based on kernel mapping, which can be seen as a particular case of a minimal partition problem, and is used as the model motivation power evolving the active contour until to catch the desired object boundary. We presented several experiments on synthetic with different noise model and real data which showed the effectiveness and the flexibility of the method.

Acknowledgments

This paper is supported by the National High-tech Research and Development Program of China (2011AA110503) and the Fundamental Research Funds for the Central Universities (T11JB00530).

References

[1] Eason G, Noble B, Sneddon I N 1995 *Phil. Trans. Roy. Soc.* **A247** 529–51
[2] Kass M, Witkin A, Terzopoulos D 1988 *Int. J. Comput. Vis.* **1**(4) 321-31
[3] Cohen L D, Cohen I 1993 *IEEE Trans. Pattern Anal. Mach. Intell* **15**(11) 1131-47
[4] Cohen L D 1991 *CVGIP: Image Understanding* **53**(2) 211-8
[5] Caselles V, Catte F, Coll T, Dibos F 1993 *Numer. Math.* **66**(1) 1-31
[6] Malladi R, Sethian J A, Vernuri B C 1995 *IEEE Trans. Pattern Anal. Mach. Intell* **17**(1) 158-75
[7] Osher S, Sethian J A 1988 *J. Comput. Phys.* **79** 12-49
[8] Caselles V, Kimmel R, Sapiro G 1997 *Int. J. Comput. Vis.* **22**(1) 61-79
[9] Yezzi A, Kichenassamy S, Kumar A, Olver P, Tannenbaum A 1997 *IEEE Trans. Med. Imag.* **16**(2) 199-209
[10] Gunn S, Nixon M 1994 *Proc. Brit. Machine Vision Conf.* 305-14
[11] Dawood M, Jiang X, Schafers K 2004 *Lecture Notes Comput. Sci.* **3212** 544-51
[12] Sorvik G 1994 *IEEE Trans. Pattern Anal. Mach. Intell.* **16**(10) 976-86
[13] Geiger D, Gupta A, Costa L A, Vlontzos J 1995 *IEEE Trans. Pattern Anal. Mach. Intell.* **17**(3) 294-302
[14] Chan T, Vese L 2001 *IEEE Trans Image Process* **10**(2) 266-77
[15] Mumford D, Shah J 1989 *Comm. Pure Appl. Math* **42** 577-685
[16] Vazquez C, Mitiche A, Ayed I B 2004 *IEEE Int. Cof. Image Processing* 3467-4370
[17] Gibou F, Fedkiw R 2005 *Proc. 4th Annu. Hawaii Int. Conf. Statistics and Mathmematics* 281-291
[18] Salah M B Mitiche A, Ayed I B 2010 *IEEE Trans. Image Precss* **19**(1) 220-32
[19] Salah M B, Mitiche A, Ayed I B 2009 *Image Process. Int. Conf.* 2997-3000
[20] Cover T M 1965 *Electron. Comput* **EC-14** 326-34
[21] Muller K R, Mika S, Ratsch G, Tsuda K, Scholkopf B 2001 *IEEE Trans. on Neur. Net.* **12**(2) 181-202
[22] Dhillon I S, Guan Y, Kulis B 2007 *IEEE Trans. Pattern Anal Mach. Intell.* **29**(11) 1944-57
[23] Wu K L, Yang M S 2002 *Pattern Recognit* **35** 2267-78
[24] Krinidis S, Chatzis V 2009 *IEEE Trans. Image. Process* **18**(12) 2747-55

Authors

Xiaofeng Li, born on February 26, 1977, Suixian Henan, China

Current position, grades: Doctor of Control Science and Engineering, lecturer and master supervisor in Beijing Jiaotong University
University studies: Control Science and Engineering in Harbin Institute of Technology (HIT)
Scientific interest: Image processing and analysis, Computer vision and Complex electromechanical system fault diagnosis
Publications:3 Patents, 10 Papers
Experience: He received Ph.D degrees on Control Science and Engineering from Harbin Institute of Technology (HIT) of China, 2008. Now he is a Lecture and master supervisor at Beijing Jiaotong University, Beijing, China. He mainly focuses on digital image processing and analysis, computer vision and complex electromechanical system fault diagnosis.

Yanfang Yang, born on August 9, 1985, Liuzhou Guangxi, China

Current position, grades: PhD Candidate
University studies: Safety Science and Engineering in Beijing Jiaotong University
Scientific interest: Image processing and analysis
Publications: 6 Papers
Experience: She is a safety science and engineering major PhD Candidate. She mainly focuses on digital image processing and analysis.

Limin Jia, born on January 18, 1963, Altai Xinjiang, China

Current position, grades: Doctor of Traffic Information Engineering & Control , professor and doctoral supervisor in Beijing Jiaotong University
University studies: Traffic Information Engineering & Control in Graduate School of China Academy of Railway Sciences
Scientific interest: Railway traffic Control and safety, intelligence transport system
Publications: 10 Patents, 100 Papers
Experience: He received Ph.D degrees on Traffic Information Engineering & Control from China Academy of Railway Sciences, 1991. Now he is a professor and doctoral supervisor in Beijing Jiaotong University. He mainly focuses on Railway traffic Control and safety, intelligence transport system